Finite Element Approximation II
MATH46052|66052 *

David J. Silvester
School of Mathematics, University of Manchester

Version 1.0 | 28 March 2019

Contents

1 A plate bending problem 1
Weak solution 2
A minimisation problem 2
2 High-order finite element approximation 3
3 A worked example 4
4 Convergence analysis 9
Quadratic convergence in energy 9

*These notes provide a summary of the essential material from the lectures. They are by no means comprehensive and should be augmented by notes taken during the lectures.

1. A plate bending problem Fourth-order differential equations have a fundamentally important role in computational solid mechanics in modelling situations where the underlying structure is extremely *thin* in one or more directions. Examples include (two-dimensional) plates and (one-dimensional) beams. The classic example of such a problem is a model of the deformation of a clamped plate under transversal loading. Thus, given a thin plate with surface Ω that is clamped at every point on its boundary $\partial\Omega$, we want to compute the deflection u at every point (x, y) when the plate is subjected to a given load function $f : \Omega \to \mathbb{R}$.[1]

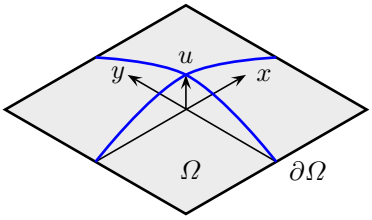

The simplest model for such a problem is the *biharmonic equation* posed over a two-dimensional domain $\Omega \subset \mathbb{R}^2$. The approximation that is discussed in detail in these notes is the *bicubic* interpolation strategy introduced earlier in the course. We will focus on a specific model problem here: given a sufficiently smooth load function f, we want to compute (or approximate) the solution function $u : \Omega \to \mathbb{R}$ satisfying

$$\nabla^2(\nabla^2 u) = f \quad \text{in } \Omega \qquad \text{(biharmonic equation)}, \tag{1.1}$$

together with the following boundary conditions:

$$u = 0 \quad \text{on } \partial\Omega \qquad \text{(zero displacement)}, \tag{1.2a}$$

$$\vec{n} \cdot \nabla u = 0 \quad \text{on } \partial\Omega \qquad \text{(zero normal derivative)}. \tag{1.2b}$$

As in part I of the notes, the starting point for a finite element analysis is the concept of a *weak solution*. This is discussed next. Once again we introduce a suitable space of "test functions", say X, and make the PDE *residual* L^2 orthogonal to all functions in this space, that is, we enforce

$$\int_\Omega \{\nabla^2(\nabla^2 u) - f\}\, v = 0 \quad \forall\, v \in X. \tag{1.3}$$

In this case we will reduce the differentiability requirements on the strong solution u satisfying (1.3) by integrating by parts *twice*. This gives

$$\int_\Omega \nabla^2(\nabla^2 u)v = \int_\Omega (\nabla^2 u)\,(\nabla^2 v) + \int_{\partial\Omega} v\,\vec{n} \cdot \nabla(\nabla^2 u)\; \mathrm{d}s - \int_{\partial\Omega} \vec{n} \cdot \nabla v(\nabla^2 u)\; \mathrm{d}s.$$

We can then simplify the formulation (remove the boundary integrals) by insisting that the test function v and its normal derivative are zero on the

[1] The thickness of the plate is assumed to remain constant during the deformation.

boundary. This gives a *weak formulation* of the clamped plate problem,

$$\int_\Omega \nabla^2 u \, \nabla^2 v = \int_\Omega f v, \tag{1.4}$$

which is required to hold for all functions v in the test space X. The specification of the weak problem is completed by identifying the largest space X for which the integrals in (1.4) remain finite. Using the Cauchy–Schwarz inequality we can show that this is precisely the space of functions that are square integrable and which have square integrable *second* derivatives. The resulting test space is thus given by

$$X = \big\{ v \,|\, v \in H^2(\Omega); v = 0, \;\; \vec{n} \cdot \nabla v = 0 \text{ on } \partial\Omega \big\}. \tag{1.5}$$

Note that the *solution space* is the same as the test space here.

(Weak solution)
A weak solution u satisfies the *essential* boundary conditions (1.2) and is the particular member of the solution space X that satisfies the weak formulation (1.4) for all functions in the test space X.

The uniqueness of the weak solution can be established by contradiction, using the Poincaré–Frieidrichs inequality applied to the test function and to its first derivative:

$$\|u\|_{L^2(\Omega)} \le L \|\nabla u\|_{L^2(\Omega)} \le L^2 \|\nabla^2 u\|_{L^2(\Omega)}, \quad u \in X, \tag{1.6}$$

where L is the length of the side of the smallest square that contains Ω.

The formulation (1.4) is equivalent to an energy *minimisation problem*.

(Minimisation problem)
Given a real function $f \in L^2(\Omega)$, and the "minimising set" X in (1.5), we seek the minimising function $u \in X$ satisfying

$$F(u) \le F(v) \quad \forall\, v \in X, \tag{1.7}$$

where $F : X \to \mathbb{R}$ is the *energy functional*

$$F(v) = \frac{1}{2} \underbrace{\int_\Omega \big(\nabla^2 v\big)^2}_{\text{I}} - \underbrace{\int_\Omega f v}_{\text{II}}. \tag{1.8}$$

Comparing with the classical formulation (1.1) and (1.2), the advantage of working with (1.7) (or the equivalent problem (1.4)) is that the energy functional is defined for very rough load data. If an infinite point load $\delta(x, y)$

is integrated against an H^2 conforming test function $v \in X$ then the second term (II) in (1.8) remains finite.[2]

Physically, the second derivatives of the displacement $\partial^2 u/\partial x^2$ and $\partial^2 u/\partial y^2$ are associated with the *bending* moment of the plate in each coordinate direction, whereas $\partial^2 u/\partial x \partial y = \partial^2 u/\partial y \partial x$ represents the *twisting* moment of the plate. Since the twisting moment plays no role in the energy functional (1.8), the first term (I) is referred to as the *bending energy*. This simplicity in the energy definition is a direct consequence of the assumed clamped plate boundary conditions, which in combination with integration by parts implies that

$$\int_\Omega \left(\frac{\partial^2 v}{\partial x\, \partial y}\right)^2 = \int_\Omega \left(\frac{\partial^2 v}{\partial x^2}\right)\left(\frac{\partial^2 v}{\partial y^2}\right) \qquad \forall\, v \in X. \tag{1.9}$$

If the weak formulation were generalised to incorporate boundary conditions consistent with a *simply supported* plate, then the energy functional (1.8) would need to be extended to include the L^2 norm of twisting moments. In this more general case, the analogue of (1.1) is referred to as the *Kirchhoff–Love* equation. Further details can be found in Braess [1, p. 324].

2. High-order finite element approximation

We will begin this section with a definition.

(Galerkin solution)
A Galerkin solution (denoted u_h) satisfies the *essential* boundary condition (1.2) and is the particular member of some (finite-dimensional) approximation space $X^h \subset X$ that satisfies a finite-dimensional version of (1.4),

$$\int_\Omega \nabla^2 u_h\, \nabla^2 v_h = \int_\Omega f v_h \quad \forall\, v_h \in X^h. \tag{2.10}$$

Next, defining the energy norm $\|u - u_h\|_E = \|\nabla^2 u - \nabla^2 u_h\|_{L^2(\Omega)}$, the *best approximation* property

$$\|u - u_h\|_E \le \|u - v_h\|_E \quad \forall\, v_h \in X^h, \tag{2.11}$$

is automatically inherited from the *Galerkin orthogonality* property (in H^2):

$$\int_\Omega \nabla^2 (u - u_h)\, \nabla^2 z_h = 0 \quad \forall\, z_h \in X^h. \tag{2.12}$$

A key question: how easy is it to construct a space X^h (that is, having square integrable second derivatives) using piecewise polynomial basis functions in two dimensions. The answer is that it is difficult. For a *conforming*

[2] Recall that a delta function is admissible as a forcing function for the Poisson problem in one dimension, but is *not admissible* in two or three dimensions.

approximation one needs to ensure C^1 continuity across element boundaries, ruling out the simple (low-order) C^0 approximations discussed in part I of the notes. In simple terms, if the approximation has kinks between elements then the plate will have infinite curvature!

(Finite element approximation)
A (conforming) finite element approximation u_h to the weak solution u satisfying (1.4) is a Galerkin solution computed using an approximation space $X_h \subset H^2(\Omega)$ that is spanned by C^1 piecewise polynomials.

The good news is that the bicubic approximation described earlier in the notes is admissible—we will use this strategy to solve a specific problem in the next section.

The difficulty in constructing a C^1 conforming approximation on an unstructured mesh of triangles has led to the development of alternative strategies, such as *nonconforming* or *mixed approximations*. An example of an admissible *nonconforming* approximation would be one that has continuous derivatives at all nodes of a triangulation, but that is not C^1 continuous at other points of the triangle edge.[3] An example of a *mixed* approximation is the *Ciarlet–Raviart* method discussed in the review paper of Glowinski and Pironneau [2]. Given a convex polygonal domain $\Omega \in \mathbb{R}^2$ and a sufficiently smooth load function f, the fourth-order equation (1.1) is decoupled into a pair of second-order equations. Thus we compute the deflection u and the bending moment ω satisfying

$$-\nabla^2 u = \omega \quad \text{in } \Omega, \tag{2.13a}$$

$$-\nabla^2 \omega = f \quad \text{in } \Omega, \tag{2.13b}$$

$$u = \frac{\partial u}{\partial n} = 0 \quad \text{on } \partial\Omega. \tag{2.13c}$$

Formulation (2.13) also arises in fluid mechanics, in which case u and ω represent the stream function and the vorticity. The obvious attraction is that both variables can be approximated using standard C^0 finite element methods. The biggest limitation is the requirement that u satisfying (2.13) is in $H^2(\Omega)$ (to ensure that (2.13a)–(2.13c) is well defined in a weak sense) which leads to a restriction in the allowable plate geometry. Another issue is that physically realistic point load functions are not admissible in this formulation.

3. A worked example Let us consider a domain Ω partitioned into n_k square elements with a total of n vertices in the interior together with n_∂ vertices on the boundary $\partial\Omega$. For example, if we were to construct a *bicubic*

[3] These methods are referred to as DKT methods (*discrete Kirchhoff triangles*); see, for example, Braess [1, pp. 328–333].

interpolant on the grid illustrated, then we would have $n = 9$ (the circled vertices) and $n_\partial = 16$ (that is, 6 vertices on a horizontal boundary, 6 on a vertical boundary, and 4 corner vertices lying on both). Then, excluding the functions interpolating the essential boundary condition from the basis, we will be left with an approximation space spanned by 64 bicubic functions in total,

$$X_h = \operatorname{span}\{\psi_k(x,y)\}_{k=1}^{64}.$$

Note that, adopting the notation introduced earlier we can decompose the set spanning X_h into 9 *nodal* functions $\psi_k(x,y) = \widehat{\phi}_i(x)\widehat{\phi}_j(y)$ (represented by the circles in the picture), 15 x-derivative functions $\psi_k(x,y) = \widetilde{\phi}_i(x)\widehat{\phi}_j(y)$ (represented by the horizontal arrows), 15 y-derivative functions $\psi_k(x,y) = \widehat{\phi}_i(x)\widetilde{\phi}_j(y)$ (represented by the vertical arrows) and 25 mixed-derivative functions $\psi_k(x,y) = \widetilde{\phi}_i(x)\widetilde{\phi}_j(y)$ (represented by the crosses).

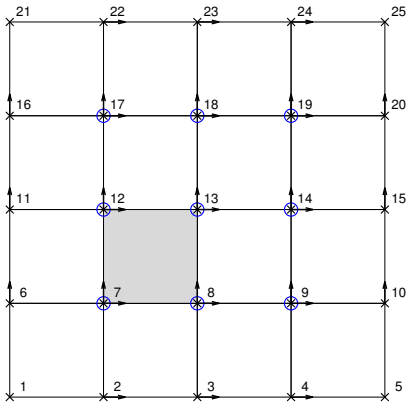

By construction, the associated finite element Galerkin solution given by $u_h(x,y) = \sum_{k=1}^{64} u_k\,\psi_k(x,y)$ is guaranteed to satisfy the essential boundary condition (1.2). Moreover, with a natural ordering, $u_1, u_2, \ldots, u_9$ will represent unknown displacement values, $u_{10}, u_{11}, \ldots, u_{39}$ will represent unknown derivative values and $u_{40}, u_{41}, \ldots, u_{64}$ will represent point values of the twisting moment. The Galerkin formulation given in (2.10),

$$\int_\Omega \nabla^2 u_h\,\nabla^2\psi_k = \int_\Omega f\psi_k, \quad k = 1,2,\ldots,64, \tag{3.14}$$

can then be written as a *Galerkin system* of linear equations

$$A\boldsymbol{u} = \boldsymbol{f}, \tag{3.15}$$

where $\boldsymbol{u}$ is the vector of the 64 unknown solution coefficients. As in part I of the notes, $A_{i,j} = \int_\Omega \nabla^2\psi_j\,\nabla^2\psi_i$ will be referred to as the *stiffness matrix*. The vector $\boldsymbol{f}_i = \int_\Omega f\psi_i$ is the associated *load vector*.

Let us focus on element ⑥ highlighted in the picture of the grid. The element contributions are given by

$$A^{⑥}_{\ell,m} = \int_{②} \nabla^2\psi_m\big|_{⑥}\,\nabla^2\psi_\ell\big|_{⑥}, \quad \ell = 1,\ldots,16,\ m = 1,\ldots,16, \tag{3.16a}$$

$$f^{②}_{\ell} = \int_{⑥} f\psi_\ell\big|_{⑥}, \quad \ell = 1,\ldots,16. \tag{3.16b}$$

The entries in the stiffness matrix can be computed analytically by considering integrals of products of the one-dimensional Hermite basis functions introduced at the strart of the course. To illustrate this construction, consider an interval $[a, b]$ of length h and define $\ell_1(s)$ and $\ell_2(s)$ to be the linear interpolation functions at the two end points as illustrated below.

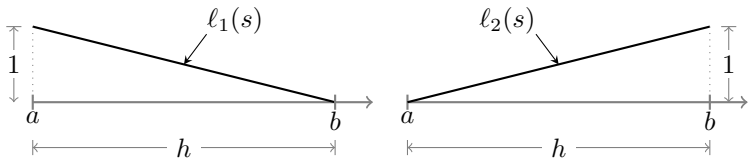

(a) (b)

The four Hermite cubic interpolation functions and their second derivatives can then be written as

$$\begin{aligned}
\widehat{\phi}_1 &= 3\ell_1^2 - 2\ell_1^3, & \widehat{\phi}_1'' &= \frac{6}{h^2}(\ell_2 - \ell_1),\\
\widehat{\phi}_2 &= 3\ell_2^2 - 2\ell_2^3, & \widehat{\phi}_1'' &= \frac{6}{h^2}(\ell_1 - \ell_2),\\
\widetilde{\phi}_1 &= h(\ell_1^2 - \ell_1^3), & \widetilde{\phi}_1'' &= \frac{2}{h}(1 - 3\ell_1),\\
\widetilde{\phi}_2 &= h(\ell_2^3 - \ell_2^2), & \widetilde{\phi}_2'' &= \frac{2}{h}(3\ell_2 - 1).
\end{aligned}$$

Products of the linear basis functions can be integrated analytically[4] and the following (one-dimensional) element matrices can then be readily computed

[4] Using the magic formula $\int_a^b \ell_1^k \ell_2^m = \frac{k!m!}{(k+m+1)!}h$.

from the component vector outer products:

$$\mathbb{M} = \int_a^b \begin{bmatrix} \widehat{\phi}_1 \\ \widehat{\phi}_2 \\ \widetilde{\phi}_1 \\ \widetilde{\phi}_2 \end{bmatrix} \begin{bmatrix} \widehat{\phi}_1 & \widehat{\phi}_2 & \widetilde{\phi}_1 & \widetilde{\phi}_2 \end{bmatrix} = \frac{h}{420} \begin{bmatrix} 156 & 54 & 22h & -13h \\ 54 & 156 & 13h & -22h \\ 22h & 13h & 4h^2 & -3h^2 \\ -13h & -22h & -3h^2 & 4h^2 \end{bmatrix},$$

$$\mathbb{A} = \int_a^b \begin{bmatrix} \widehat{\phi}_1'' \\ \widehat{\phi}_2'' \\ \widetilde{\phi}_1'' \\ \widetilde{\phi}_2'' \end{bmatrix} \begin{bmatrix} \widehat{\phi}_1'' & \widehat{\phi}_2'' & \widetilde{\phi}_1'' & \widetilde{\phi}_2'' \end{bmatrix} = \frac{2}{h^2} \begin{bmatrix} 6 & -6 & 3h & 3h \\ -6 & 6 & -3h & -3h \\ 3h & -3h & 2h^2 & h^2 \\ 3h & -3h & h^2 & 2h^2 \end{bmatrix},$$

$$\mathbb{L} = \int_a^b \begin{bmatrix} \widehat{\phi}_1'' \\ \widehat{\phi}_2'' \\ \widetilde{\phi}_1'' \\ \widetilde{\phi}_2'' \end{bmatrix} \begin{bmatrix} \widehat{\phi}_1 & \widehat{\phi}_2 & \widetilde{\phi}_1 & \widetilde{\phi}_2 \end{bmatrix} = 30h \begin{bmatrix} -36 & 36 & -3h & -3h \\ 36 & -36 & 3h & 3h \\ -33h & 3h & -4h^2 & h^2 \\ -3h & 33h & h^2 & -4h^2 \end{bmatrix}.$$

The matrix $\mathbb{M}$ is the cubic Hermite basis *mass* matrix, $\mathbb{A}$ is the one-dimensional *stiffness* matrix and $\mathbb{L}$ is the *connection* matrix. In the specific case of a constant load function $f = 1$, the one-dimensional *load* vector is given by

$$\mathbb{ff} = \int_a^b \begin{bmatrix} \widehat{\phi}_1 \\ \widehat{\phi}_2 \\ \widetilde{\phi}_1 \\ \widetilde{\phi}_2 \end{bmatrix} = \frac{h}{12} \begin{bmatrix} 6 \\ 6 \\ h \\ -h \end{bmatrix}$$

To construct the two-dimensional stiffness matrix $A^{\textcircled{k}}$ we first map the one-dimensional basis functions in x and y into the two-dimensional basis set. Typically, the 16 element basis functions on element $\textcircled{k}$ will be ordered naturally, so that the nodal functions come first and the mixed-derivative functions come last. Specifically, if the mapping vectors are given by

$$\mathtt{x} = [1, 2, 2, 1, 3, 4, 4, 3, 1, 2, 2, 1, 3, 4, 4, 3],$$
$$\mathtt{y} = [1, 1, 2, 2, 1, 1, 2, 2, 3, 3, 4, 4, 3, 3, 4, 4],$$

and if we define the vectors

$$\boldsymbol{\phi}_{\mathtt{x}}(x) = \begin{bmatrix} \widehat{\phi}_1(x) \\ \widehat{\phi}_2(x) \\ \widetilde{\phi}_1(x) \\ \widetilde{\phi}_2(x) \end{bmatrix}, \quad \boldsymbol{\phi}_{\mathtt{y}}(y) = \begin{bmatrix} \widehat{\phi}_1(y) \\ \widehat{\phi}_2(y) \\ \widetilde{\phi}_1(y) \\ \widetilde{\phi}_2(y) \end{bmatrix},$$

we can construct local basis functions via $\psi_k(x, y) = \boldsymbol{\phi}_{\mathtt{x}_\mathtt{i}}(x)\, \boldsymbol{\phi}_{\mathtt{y}_\mathtt{j}}(y)$. The

element integration can then be separated, so that, for example

$$\int_{\mathbb{k}} \psi_i(x,y)\,\psi_j(x,y) = \Big\{ \int_{x_{k-1}}^{x_k} \boldsymbol{\phi}_{\mathtt{x}_i} \boldsymbol{\phi}_{\mathtt{x}_j} \Big\} \Big\{ \int_{y_{k-1}}^{y_k} \boldsymbol{\phi}_{\mathtt{y}_i} \boldsymbol{\phi}_{\mathtt{y}_j} \Big\} = \mathbb{M}_{\mathtt{x}_i,\mathtt{x}_j}\, \mathbb{M}_{\mathtt{x}_i,\mathtt{x}_j}.$$

This motivates the construction of extension matrices $\mathbb{M}_{\mathtt{x},\mathtt{x}}$, $\mathbb{M}_{\mathtt{y},\mathtt{y}}$, $\mathbb{A}_{\mathtt{x},\mathtt{x}}$, $\mathbb{A}_{\mathtt{y},\mathtt{y}}$, $\mathbb{L}_{\mathtt{x},\mathtt{x}}$, $\mathbb{L}_{\mathtt{y},\mathtt{y}}$, each having 16 rows and 16 columns, from the component matrices $\mathbb{M}$, $\mathbb{A}$ and $\mathbb{L}$. Thus, given the indexing vectors $\mathtt{x}$ and $\mathtt{y}$ above, the (5,11) element of matrix $\mathbb{L}_{\mathtt{x},\mathtt{x}}$ is $30h \cdot 3h$ (the (3,2) entry of $\mathbb{L}$). Similarly, the (4,6) element of matrix $\mathbb{A}_{\mathtt{y},\mathtt{y}}$ is given by $-12/h^2$.

The bicubic stiffness matrix $A^{\mathbb{k}}$ is then readily computed as the following sum of *Hadamard* (entrywise) products of the extended matrices:[5]

$$A^{\mathbb{k}} = \mathbb{A}_{\mathtt{x},\mathtt{x}} \circ \mathbb{M}_{\mathtt{y},\mathtt{y}} + \mathbb{L}^T_{\mathtt{x},\mathtt{x}} \circ \mathbb{L}_{\mathtt{y},\mathtt{y}} + \mathbb{L}_{\mathtt{x},\mathtt{x}} \circ \mathbb{L}^T_{\mathtt{y},\mathtt{y}} + \mathbb{M}_{\mathtt{x},\mathtt{x}} \circ \mathbb{A}_{\mathtt{y},\mathtt{y}}.$$

The element load vector $f^{\mathbb{k}}$ has the analogous construction

$$f^{\mathbb{k}} = \mathit{ff}_{\mathtt{x}} \circ \mathit{ff}_{\mathtt{y}}.$$

Returning to the grid illustrated at the beginning of this section, the element contributions (3.16) are given by setting $h = 1/2$ above. The uniform grid and the constant load f imply that the element matrices and element load vectors are identical. The entries in the element stiffness matrix (truncating to 4 decimal digits) and the element load vector are given by

$$A^{\textcircled{6}} = \begin{bmatrix} 47.1771 & -23.1771 & \cdots & 0.2486 \\ \vdots & \vdots & & \vdots \\ 0.2486 & 0.3514 & \cdots & 0.0279 \end{bmatrix}, \quad f^{\textcircled{6}} = \begin{bmatrix} 1/16 \\ \vdots \\ -1/2304 \end{bmatrix}.$$

As expected, the matrix $A^{\textcircled{6}}$ is *dense*: that is, all 256 entries in the matrix are nonzero. After assembling the 16 element contributions, the 64×64 Galerkin system (3.15) can be solved to give the coefficients $u_7 = u_9 = u_{17} = u_{19} = 0.00865$, $u_8 = u_{12} = u_{14} = u_{18} = 0.01399$ and $u_{13} = 0.02272$. The last number represents the displacement at the centre of the plate. The associated Galerkin solution is given by

$$u_h(x,y) = 0.00865\,\psi_7(x,y) + \cdots + 0.02272\,\psi_{13}(x,y) + \cdots + 0.18820\,\psi_{64}(x,y).$$

Note that the final value $u_{64} = 0.18820$ represents the twisting moment of the plate at the top corner point (1,1).

The figure illustrates the bicubic finite element solution to the uniformly loaded plate problem computed using a refined 64×64 subdivision. The

[5] Using MATLAB the code to generate the element stiffness matrix is very compact:

```
AK = AA(x,x).*MM(y,y) +LL(x,x)'.*LL(y,y) +LL(x,x).*LL(y,y)' +MM(x,x).*AA(y,y);
```

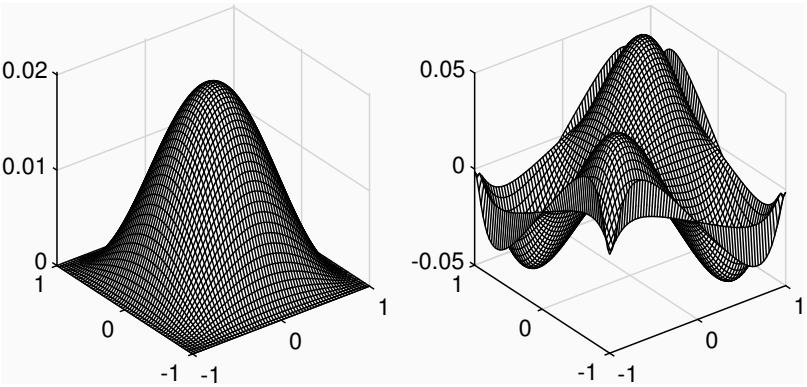

displacement profile shown on the left is visually smooth and has the expected lines of symmetry: the two coordinate axes and the lines $y = x$ and $y = -x$. As expected, the maximum computed displacement is at the centre of the plate $u_h(0, 0) = 0.020247$. The computed solution is positive everywhere except at the points nearest the four corners where a small negative displacement value is computed. This is not a numerical instability—we will expand on this point below. The twisting moment shown on the right has an oscillatory structure with two positive peaks and two negative peaks. The computed solution is symmetric about the line $y = x$ and the line $y = -x$. As might be anticipated, it is *antisymmetric* with respect to the two coordinate axes, so the computed value of $\partial^2 u_h/\partial x \partial y$ at the origin is zero.

4. Convergence analysis How accurate is the finite element approximation? To answer this we need to simply repeat the steps of the error analysis part I of the notes. Doing so gives the following a priori error estimate of the error in the energy norm.

(Quadratic convergence in energy)
If the weak solution $u \in X$ of (1.1)–(1.2) is smooth enough, that is, if $u \in H^4(\Omega)$, then the bicubic finite element function u_h solving (2.10) on a grid of square elements satisfies the *energy error* bound

$$\|u - u_h\|_E \leq C_4\, h^2, \tag{4.17}$$

where h is the edge length and the constant C_4 depends only on $\|\,\mathrm{D}^4 u\|_{L^2(\Omega)}$.

To investigate this, selected point values of the computed solutions are listed in the following table. These results were generated by solving the uniformly loaded plate problem on a sequence of finer and finer grids. Looking at these numbers, each successive refinement of the grid can be seen to give

an additional digit of accuracy in the displacement solution at the centre of the plate. From a theory perspective, one might expect that the error in the displacement value $u_h(0,0)$ will exhibit fourth-order convergence when $h \to 0$. This convergence rate is unlikely to be attained in practice however. For the problem of interest, the corners of the plate generate (weak) singularities in the solution so that $u \notin H^4(\Omega)$. This explains why the differences between successive estimates of $u(0,0)$ are consistent with an error reduction rate proportional to h^3 rather than h^4.

h	$u_h\big\vert_{(0,0)}$	$\frac{\partial^2 u_h}{\partial x\,\partial y}\big\vert_{(1,1)}$	λ_h^1	Ratio
$1/2$	0.022716	1.8820×10^{-1}	10.8743	—
$1/4$	0.020803	1.1325×10^{-1}	43.2815	—
$1/8$	0.020333	4.1581×10^{-2}	80.5516	—
$1/16$	0.020257	1.0344×10^{-2}	80.8792	7.04
$1/32$	0.020247	1.3733×10^{-3}	80.9262	7.54
$1/64$	0.020245	-1.7123×10^{-4}	80.9325	8.00
$1/128$	0.020245	-1.5409×10^{-4}	80.9333	8.00
$1/\infty$	0.020245		80.9334	

The convergence of the computed solution to the twisting moment at the corner is much more erratic. Looking at these numbers we can make two observations. First, when the grid resolution is fine enough ($h \leq 1/64$) the negative displacements that are computed in the vicinity of the four corners lead to a change of sign in the computed moment. Second, the point values tabulated do not seem to be converging to a limit value when $h \to 0$.

The other set of numbers λ_h^1 listed in the table are estimates of the smallest eigenvalue λ^1 of the biharmonic operator on the square domain Ω. This value is the smallest number $\lambda \in \mathbb{R}$ for which one can find a corresponding function $u : \Omega \to \mathbb{R}$ (with $u \neq 0$) that satisfies

$$\nabla^2(\nabla^2 u) = \lambda u \quad \text{in } \Omega, \tag{4.18a}$$

$$u = \frac{\partial u}{\partial n} = 0 \quad \text{on } \partial\Omega. \tag{4.18b}$$

This eigenvalue problem arises when one is investigating the resonant modes of vibration of the clamped plate from a computational perspective. The corresponding eigenfunctions u^j, $j = 1, 2, \ldots$ represent these modes. The value λ^1 has particular significance in engineering applications since it is associated with the *fundamental frequency* of oscillation. The sequence of estimates λ_h^1 in the table were computed by solving the discrete (generalised) eigenvalue problem

$$A\boldsymbol{x} = \lambda_h M\boldsymbol{x} \tag{4.19}$$

at each grid level. Here A is the stiffness matrix in (3.15) and M is the corresponding *mass matrix* $M_{i,j} = \int_\Omega \psi_j \, \psi_i$. This matrix can also be assembled from element matrices by taking the product of one-dimensional matrices, specifically, $\mathbb{M}_{\mathtt{x},\mathtt{x}} \circ \mathbb{M}_{\mathtt{y},\mathtt{y}}$. Looking at the table, the computed estimates λ_h^1 can be seen to converge to a well-defined limit. The final column in the table gives the ratio $(\lambda^1 - \lambda_h^1)/(\lambda^1 - \lambda_{h/2}^1)$. Since $8 = 2^3$ these numbers are consistent with third-order convergence of λ_h^1 to λ^1 as $h \to 0$.

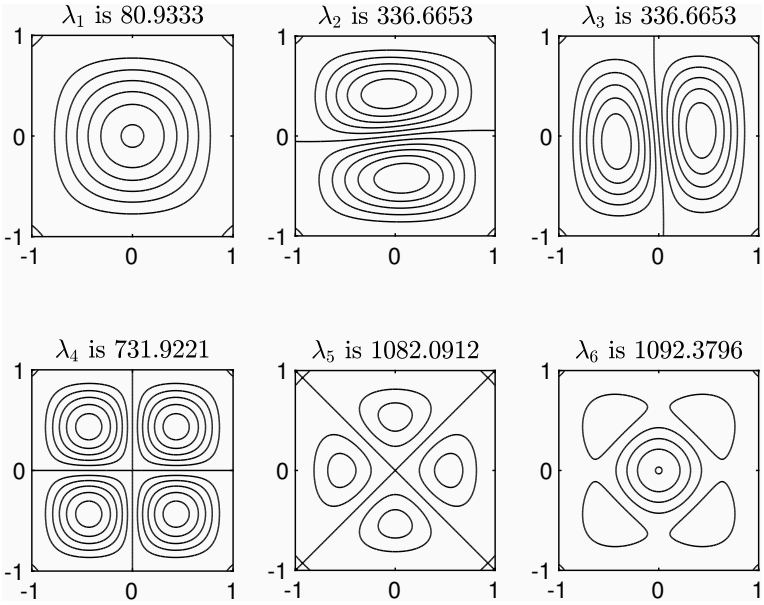

Contour plots of the first six eigenfunctions (computed on the finest grid) are shown in the figure. Once again we can see interesting behaviour in the four corners of the plate. These local features are associated with the regions of sign oscillation and in a fluid mechanics setting they are referred to as *Moffatt vortices*.[6]

The computational results presented above can be reproduced using the IFISS package: `http://www.manchester.ac.uk/ifiss/` and, in particular, by running the driver `square_plate`.

[6]The fundamental mode of the Laplacian operator is positive (or negative) everywhere in Ω. The biharmonic modes all have an infinite sequence of sign changes in the corners!

References

[1] Dietrich Braess. *Finite elements*. Cambridge University Press, Cambridge, 2007. Third edition, ISBN: 978-0-521-70518-9.

[2] Roland Glowinski and Olivier Pironneau. Numerical methods for the first biharmonic equation and for the two-dimensional Stokes problem. *SIAM Review*, 21:167–212, 1979. doi: 10.1137/1021028.